Chemistry & Biology, Vol. 11, 525–534, April, 2004, ©2004 Elsevier Science Ltd. All rights reserved. DOI 10.1016/j.chembiol.2004.03.022

Structural Determinants of CDK4 Inhibition and Design of Selective ATP Competitive Inhibitors

Campbell McInnes,* Shudong Wang, Sian Anderson, Janice O'Boyle, Wayne Jackson, George Kontopidis, Christopher Meades, Mokdad Mezna, Mark Thomas, Gavin Wood, David P. Lane, and Peter M. Fischer
Cyclacel Limited
James Lindsay Place
Dundee Technopole
Dundee DD1 5JJ
United Kingdom

Summary

A number of selective inhibitors of the CDK4/cyclin D1 complex have been reported recently. Due to the absence of an experimental CDK4 structure, the ligand and protein determinants contributing to CDK4 selectivity are poorly understood at present. Here, we report the use of computational methods to elucidate the characteristics of selectivity and to derive the structural basis for specific, high-affinity binding of inhibitors to the CDK4 active site. From these data, the hypothesis emerged that appropriate incorporation of an ionizable function into a CDK2 inhibitor results in more favorable binding to CDK4. This knowledge was applied to the design of compounds in the otherwise CDK2-selective 2-anilino-4-(thiazol-5-yl)pyrimidine pharmacophore that are potent and highly selective ATP antagonists of CDK4/cyclin D1. The findings of this study also have significant implications in the design of CDK4 mimic structures based on CDK2.

Introduction

The cyclin-dependent kinases (CDKs) are key regulators of progression through the various stages of the eukaryotic cell cycle [1, 2]. It has been shown that overexpression and/or loss of function of key proteins implicated in the chain of events upstream and downstream of the CDKs leads to tumorigenesis and neoplastic transformation [3]. This includes the cyclins (positive regulatory subunits), the natural inhibitory proteins, $p16/p19^{INK4}$, $p21^{WAF1}$, and $p27^{KIP1}$, as well as the downstream targets of CDK phosphorylation, i.e. the retinoblastoma protein (pRb) and the E2F family of transcription factors. In each case, pharmacological inhibition of CDK activity should lead to restoration of the cell cycle checkpoints and potentially trigger cell death via apoptosis [4]. It can thus be seen that these enzymes represent interesting pharmaceutical targets, since tumors arising from a number of different gene mutations could be treated by using kinase inhibitors specific for the CDKs. While at present at least nine CDK isoforms have been identified and characterized, the main focus of CDK-based cancer therapy to date has been on CDK4 and CDK6/cyclin D (G1 phase), CDK2/cyclin A and CDK2/cyclin E (G1 and S phases), and CDK1/cyclin B (G2/M phases). The primary strategy for CDK inhibition has been to develop small molecules that compete with ATP for binding to the kinase. However, an alternative approach currently being investigated is to block recruitment of macromolecular substrates to the complex [5]. While there are numerous examples of very potent ATP competitive inhibitors of CDK2 and CDK4 [6–8], very few compounds have progressed past the preclinical stage [9]. Hence, there remains tremendous scope for further development of new classes of CDK inhibitors, especially those that target the individual kinase isoforms specifically. Selective inhibitors might be expected to be generally less cytotoxic and perhaps to exhibit a better side effect profile. CDK4/cyclin D1 has been demonstrated to play critical roles during initiation of cell division in quiescent cells (G0/G1 transition) and cell cycle commitment at the restriction point in G1. Furthermore, CDK4 and CDK6 are frequently direct or indirect targets of genetic alterations in cancer and are amplified or overexpressed in a variety of tumors [10]. Cyclin D-dependent kinases are therefore thought to represents viable targets for antitumor therapy, as kinase inhibition would prevent cell proliferation via maintenance of hypophosphorylated pRb, which remains complexed with E2F1/DP1, thereby preventing transcription of genes necessary for the progression into the S phase of the cell cycle [11–13].

There have been numerous reports of ATP-competitive compounds that bind selectively to CDK4 and attempts at optimizing their binding and specificity for individual kinase isoforms by using structure-based design methods [14–21]. However, there has been little discussion of the factors, from both the inhibitor and protein perspectives, contributing to CDK4 potency and selectivity. Here, we report a comprehensive study of known selective inhibitors of CDK4 and describe the structural basis for their preferential inhibition over CDK2. We have constructed a homology model of CDK4 and used this model in order to dock structures of published inhibitors. The structural determinants for CDK4 inhibition observed from these calculations were then applied in order to guide the tailoring of the otherwise CDK2-selective 2-anilino-4-(thiazol-5-yl)pyrimidine pharmacophore [22] to produce the first compounds in this series with CDK4/cyclin D1 selectivity.

Results and Discussion

Generation and Validation of the CDK4 Homology Structure

To date, there have been a number of CDK inhibitory compounds described that bind preferentially to CDK4; however, no significant progress in determining the features required for selectivity toward CDK4 has been reported. A major reason for this lack of insight has been the paucity of structural information for this CDK isoform. In contrast, there is a plethora of structural data

*Correspondence: cmcinnes@cyclacel.com

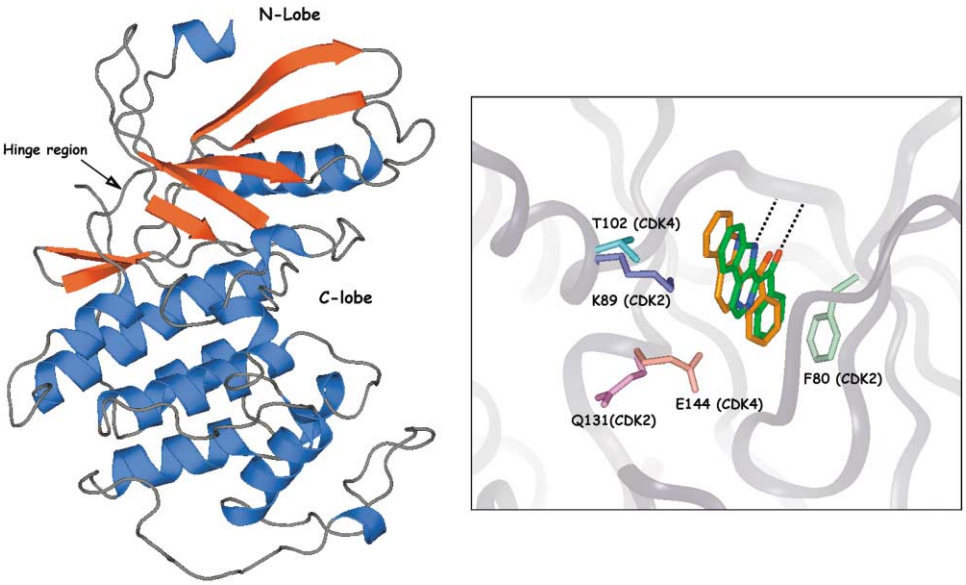

Figure 1. Homology Model of CDK4 and Docking of a Selective Inhibitor

(A) Ribbon diagram [29] for the homology structure generated for CDK4 based on sequence comparisons with the X-ray structures of CDK2 and CDK6. This figure illustrates the topology of protein kinase domains.

(B) Superposition of the models of Fascaplysin within the ATP binding sites of CDK2 and CDK4 generated by docking with Affinity (Insight2000, Accelrys). The CDK2 docked ligand is colored with green carbon atoms, whereas the CDK4 ligand is in brown. Only the backbone ribbon of CDK4 is shown along with the major residues differing in the two proteins. $F80^{CDK2}$ and the hinge region H bonds are shown as reference points. The position of $E144^{CDK4}$ is induced by electrostatic interaction with the ligand.

for CDK2, as it has been crystallized successfully in many forms, including monomeric and cyclin A-activated forms in free and inhibitor bound complexes. Until now, two approaches have been used to obtain structural information and to generate binding modes for CDK4 inhibitory molecules. These include (1) structures derived from sequence homology with other CDKs [20, 21] and (2) crystallization of monomeric CDK2, where the residues differing in the ATP binding pocket were replaced with the corresponding residues of the CDK4 active site [23]. We have employed the homology modeling approach in conjunction with automated flexible docking methods to generate a set of binding hypotheses for the ligand-CDK4 complexes of a number of published inhibitors.

The homology structure of CDK4 in the present study was generated by using CDK2 and CDK6 as template structures, since there are differing regions in both proteins that possess high sequence identity with CDK4 (Figure 1A). Before its use as the basis for further docking simulations with CDK4-selective compounds, the model was validated though docking of 4-[4-(2,4-dimethyl-thiazol-5-yl)pyrimidin-2-ylamino]phenol, a compound that is approximately equipotent against CDK2 and CDK4 [24]. The poses obtained for this inhibitor were shown to be almost identical in the two ATP binding sites (with only slight differences in the positioning of the hydroxyanilino ring). This similarity was also confirmed by comparison of the energetics of binding, which correlate well with the equipotent IC_{50}'s of this compound against CDK2/A and CDK4/D1. In addition, the CDK2 docked structure overlaid closely with the crystal structure [24]. These results therefore confirmed that the model was correct and demonstrate its utility for further calculations.

Based on analysis of the nature and sequence of the residues lining the ATP binding pocket, it was possible to determine the specific residues and side chains that differ in the CDK4 structure with respect to CDK2 and to identify the interactions that could be exploited in the design of selective compounds. This information could be used in two ways, both in the enhancement of CDK4 selectivity and in the engineering of molecules with reduced binding to CDK4 and higher specificity for CDK2. The residues comprising the ATP cleft of both CDK2 and CDK4 are compared in Table 1. As can be seen, the key differences concern residues $T102^{CDK4}$ (found on the CDK "specificity surface") and $E144^{CDK4}$ (which contact the phosphates of ATP [CDK2 analogy]). The other changes include the $H95^{CDK4}$ and $V96^{CDK4}$ replacements for the hinge region H bonding-interacting residues. As these residues provide contacts through the backbone, they would not be expected to impact inhibitor binding significantly. The composition of the two binding pockets thus differs due to the nonconservative changes in key ATP- and inhibitor-contacting residues.

Molecular Basis for CDK4 Selectivity of Published ATP Inhibitor Structures

As is summarized in Table 2, several compounds that exhibit preferential binding to CDK4 over CDK2 have been described in the literature to date. These include fascaplysin [20], NSC625987 [19], PD0183812 [14, 25], and the urea-based inhibitors reported recently [17, 18, 23]. In order to determine the molecular basis for the selectivity of these compounds in terms of their interac-

Table 1. Comparison of the ATP-Contacting Residues in CDK2 and CDK4

	10	18	31	64	80	81	82	83	85	86	89	131	134	144	145
CDK2	Ile	Val	Ala	Val	Phe	Glu	Phe	Leu	Gln	Asp	Lys	Gln	Leu	Ala	Asp
	Ile	Val	Ala	Val	Phe	Glu	**His**	**Val**	Gln	Asp	**Thr**	**Glu**	Leu	Ala	Asp
CDK4	12	20	33	77	93	94	95	96	98	99	102	144	147	157	158

tions with the residues comprising the ATP binding pocket, the structure of each was used in molecular docking experiments with the X-ray structure of CDK2 and with the model structure of CDK4. The first compound studied was the natural product fascaplysin, which was recently described and shown to inhibit CDK4/D1 with an IC_{50} of 0.35 μM, without appreciable activity on CDK2/E [20]. The structural basis for selectivity of this inhibitor was not immediately apparent from examination of its docked poses in CDK2 and CDK4. Fascaplysin, which contains a quaternary nitrogen at the intersection of two of its aromatic rings, binds in a similar conformation in both cases with the lactam NH and carbonyl groups forming a donor-acceptor hydrogen bond pair to the hinge region ($L83^{CDK2}$ [$V96^{CDK4}$]) as shown in Figure 1B. Such an interaction involving the backbone connecting the N- and C-terminal kinase domain lobes is observed with all CDK2 inhibitors and many other kinase ATP antagonists. Relative to the CDK4 binding mode, the CDK2-docked structure projects slightly further into the base of the ATP cleft and hence makes more complementary van der Waals contacts with $V18^{CDK2}$, $F80^{CDK2}$, and $L134^{CDK2}$, which is reflected in the more favorable vdW interaction energy (Table 2). The contribution of the Coulombic term to the enthalpy of binding, on the other hand, was strikingly different between CDK2 and CDK4 (+28 versus −60 kcal/mol, respectively) and resulted in a much more favorable energy for binding to CDK4 (−86 kcal/mol more favorable). The difference in nonbonded energies correlates well with the observed potency differences (fascaplysin is at least 100-fold more active against CDK4) and examination of the catalytic sites of both enzymes explains the structural basis for the variation. In CDK4, an acidic residue (E144) replaces $Q131^{CDK2}$, whereas a neutral residue ($T102^{CDK4}$) is substituted for the positively charged $K89^{CDK2}$. These differences lead to a two-unit increase in the formal charge of the ATP binding pocket of CDK2 relative to CDK4 and explain the more favorable electrostatic energy with the latter kinase. The quater-

Table 2. In Vitro Activity, Calculated pK_a, and Energetic Data for Reported CDK4-Selective Inhibitors

Inhibitor		CDK			Interaction Energy (kcal/mol)		
Number	Name	Isoform	IC_{50} (μm)	pK_a (calculated)	Total	van der Waals	Coulombic
1	Fascaplysin	4	0.35	–	−88.1	−28.6	−60.1
		2	>50		−1.6	−30.1	28.5
2	PD0183812	4	0.008	7	−115.3	−77	−38.3
		2	0.165		−30.9	5.5	−36.4
3	NSC625987	4	0.2	0.5	−31.4	−28.6	−4.6
		2	>100		–	–	–
4	Pyrazol-3-yl urea	4M2	1.6	10.3	−32.1	−30.5	−1.6
		4	0.2		−54.2	−33.8	−20.4
		2	25		−28.8	−29	0.2
5	Pyridin-2-yl urea	4M2	0.051	–	−26.5	−21.8	−4.7
		2	0.096		−41.8	−32.2	−9.6

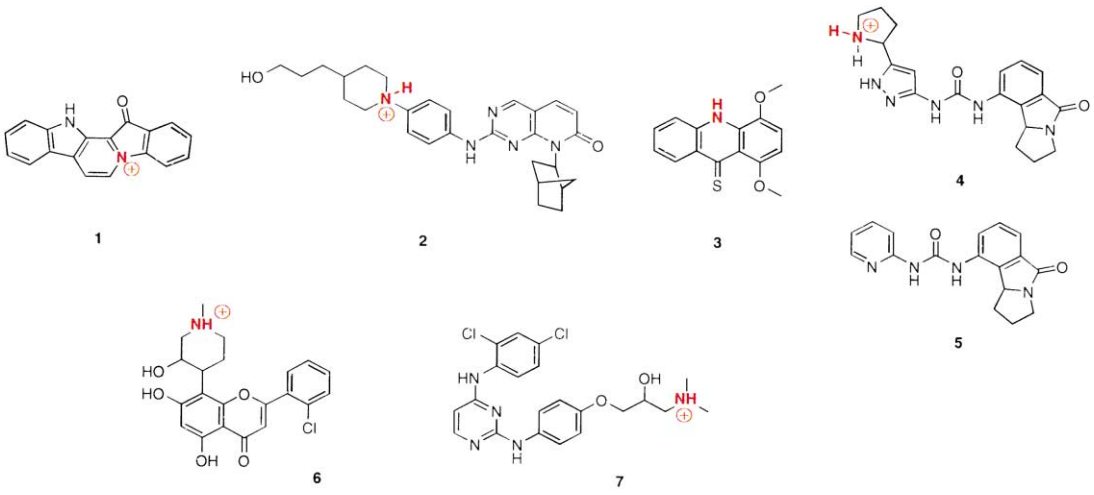

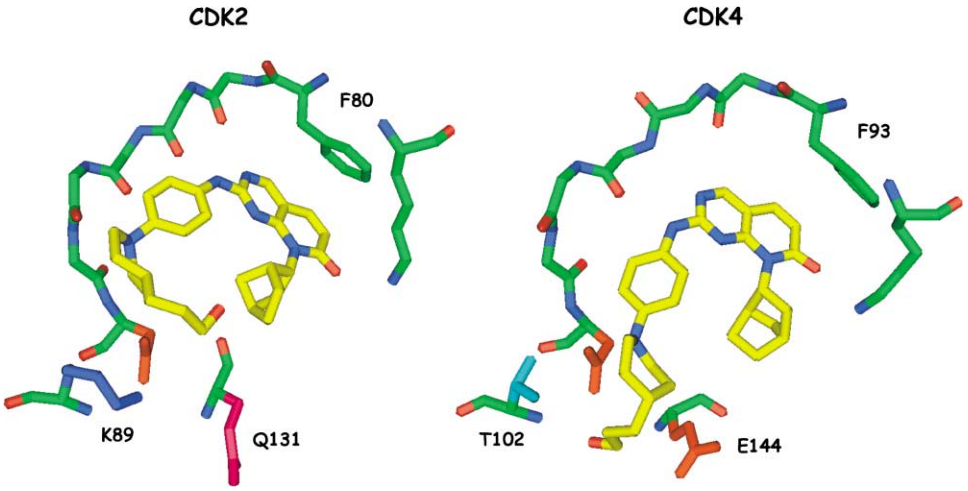

Figure 2. Comparison of the Interactions of PD013812 with CDK2 and CDK4 Based on their Affinity-Modeled Structures

Residues of the ATP binding pocket differing and thus contributing to CDK4 (right) selectivity are labeled. The CDK2 (left) pose is more compact as a result of a steric clash with K89.

nary nitrogen of fascaplysin is in close proximity to E144^{CDK4}, resulting in the increased contribution to the Coulombic term. Additionally, the proximity of the ligand quaternary N to K89^{CDK2} leads to less favorable binding to CDK2. Interestingly, the steric constraint of the larger K89^{CDK2} side chain (salt bridged to D86^{CDK2}) results in contacts with the lipophilic rings of fascaplysin and also in better complementarity with the lipophilic part of the cleft relative to CDK4 (as shown by the more favorable vdW interaction energy; Table 2); however, this in turn results in weaker H bonding with the CDK2 hinge region (as shown by Ludi H bonding scores of 62 for CDK2 versus 78 for CDK4). The combination of less-optimal H bonds and unfavorable electrostatic interactions thus offsets the increase in vdW energy and results in the two orders of magnitude decrease in potency of fascaplysin against CDK2 compared to CDK4. As D86^{CDK2} (D99^{CDK4}) is invariant between the two kinases, it makes equal, although important, contacts in both cases. Although a CDK2-based homology model of CDK4 was presented in the original report on fascaplysin [20], no mention was made of the structural basis for the observed CDK selectivity. Fascaplysin was also reported in that study to have a 10-fold lower potency against CDK6. This result is in line with the above discussion, as the residue in CDK6 corresponding to E144^{CDK4} is Q149 and thus identical to CDK2 in this position.

The highly selective compound, PD0183812 (20-fold selective for CDK4) [14], was subsequently modeled into the binding sites of the CDK4 and CDK2 models. The correctness of the docked CDK2 complex was ascertained by comparison with the described interactions of a compound closely related to PD0183812 with CDK2 [14]. PD0183812 possesses at least one ionizable nitrogen that is potentially protonated at physiological pH, and the calculated pK_a value for the piperidine N was found to be 7.0. This suggests that this molecule would be appreciably protonated under the conditions of the assay. Flexible docking of the protonated inhibitor into the CDK4 active site again generated a similar pose to that observed with CDK2. As observed with fascaplysin, examination of the ligand-protein nonbonded energies revealed significantly more favorable binding free energies with CDK4 (−115 kcal/mol versus −31 for CDK2), mostly as a result of the additional electrostatic contribution from the charged nitrogen to E144^{CDK4} (Table 2). Again the role of K89^{CDK2} results in more complementary contacts of the inhibitor with the interior of the cleft; however, it is also more compact and folds up on itself (Figure 2). This advantage is offset in the CDK4 context by a more extended conformation of the ligand and resulting contacts with T102^{CDK4} replacing K89^{CDK2}, leading to more favorable vdW interaction energies with CDK4 as a whole. In addition, for the CDK2 bound inhibitor, the observed hinge region H bonds are more optimal (to Leu83^{CDK2}) than those made to the corresponding backbone atoms of V96^{CDK4} (as evidenced by the H bond Ludi complementarity score of 349 versus 279). This is probably a consequence of the steric constraint of K89^{CDK2} inducing a compacting of the inhibitor and wedging it further into the cleft. The advantage provided by the increase in H bonding complementarity is countered by the charge-charge repulsion of the quaternary nitrogen, resulting in the observed selectivity of PD0183812. As additional evidence for the contribution of the charge to CDK4 binding of the series of compounds reported [14], only those containing a positively charged N were selective for CDK4.

The CDK4-selective 10*H*-acridine-9-thione NSC625987 was also modeled on a comparative basis with the ATP clefts of both CDK isoforms (Figure 3). This compound contains three fused aromatic rings and was reported to have at least a 500-fold selectivity for CDK4 [19]. While this inhibitor possesses an ionizable N, its pK_a is well below neutral pH (calculated pK_a ~0.5). The compound is therefore essentially uncharged under physiological conditions. The selectivity of NSC625987 thus mostly results from the differing contacts and side chain orientations in CDK4. Molecular docking of NSC645787 with CDK2 did not result in a binding mode consistent

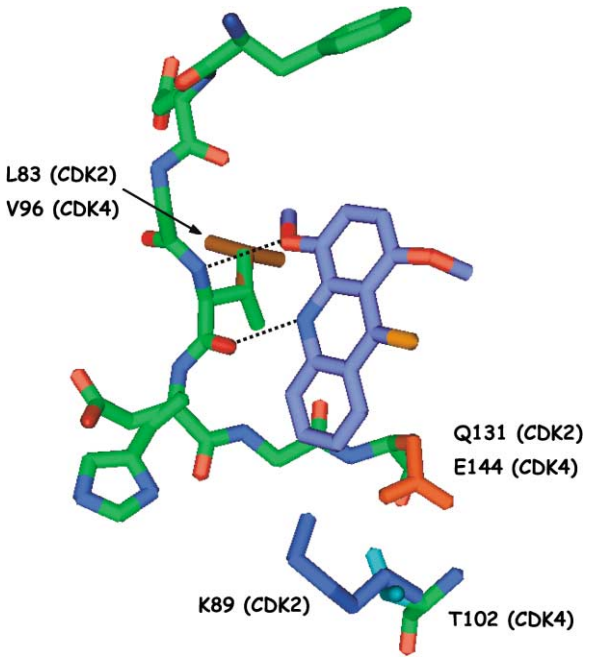

Figure 3. The Modeled CDK4 Binding Mode of NSC625987 Generated by Molecular Docking

The differing side chains of CDK2 are labeled in addition to the corresponding side chains and backbone atoms of CDK4. The smaller V96 (partial brown) and T102 residues of CDK4 result in greater flexibility of the hinge region and more volume in the ATP binding site, allowing NSC625987 to bind.

with known determinants of CDK inhibitor binding. The modeled pose with CDK4, however, was suggestive of CDK inhibition, with an appropriate H bond from the ligand NH to the $V96^{CDK4}$ carbonyl (Figure 3). The observation that this inhibitor is not predicted to bind with known kinase inhibitory contacts is consistent with its inactivity toward CDK2. The lack of binding most probably results from its inability to make effective H bonds to the backbone of CDK2. The constraint imposed by the side chain of $K89^{CDK2}$ in conjunction with the more bulky phenyl ring ($F82^{CDK2}$) in the CDK2 binding pocket ($H95^{CDK4}$) displaces these contacts and precludes overall complementary interactions with the ATP cleft. The larger volume and additional flexibility of the backbone (due to the smaller $V96^{CDK4}$ side chain) in the CDK4 active site enables high-affinity binding of NSC625987.

A recent study by Banyu Tsukuba/Merck described the structure-based design of CDK4 selective inhibitors by using several approaches [17, 18, 23]. A de novo design algorithm was used to identify ATP-competitive molecules, and this was followed by design through the use of a homology structure. This group were also the first to describe a mutagenesis strategy whereby CDK2 was used as a scaffold, and the differing residues in the ATP binding site were replaced with the corresponding residues of CDK4. This construct was validated by using an in vitro kinase assay to demonstrate that while CDK4-selective compounds were less potent against the CDK4 mimic CDK2 (CDK4M2), the rank order of selectivity was preserved. This scaffold was then used to determine the complex structure of the CDK4-specific bisarylurea compounds described (Table 2). Of the inhibitors described, those that bind preferentially to CDK4 again contain protonated Ns, whereas those with little or no selectivity do not contain this postulated determinant. Despite the structural difference and the resulting effect on the structure-activity relationship, no mention was made of this feature, and few other details contributing to CDK4 selectivity were discussed. To test our hypothesis regarding CDK4 selectivity depending on the presence of appropriate cationic groups in the inhibitors, further energetic calculations were performed on the relevant crystal structures deposited in the protein databank, in conjunction with docking calculations to generate structures not generated or disclosed. Two compounds were examined that were reported as selective and nonselective inhibitors of CDK4 with respect to CDK2. The first (**4**, Table 2) was a pyrazol-3-yl urea (CDK4 selective) containing a charged group, and the second was a pyridin-2-yl urea (**5**, Table 2; equipotent) without the latter functionality. The complex of **4** with the CDK4M2, in which the residues of the CDK4 ATP pocket were placed in the CDK2 frame, was deposited in the protein databank. To determine the molecular basis of selectivity, this compound was docked with CDK2. Calculation of the intermolecular inhibitor-CDK interaction energies surprisingly did not show a marked difference between the CDK2 and CDK4 complexes as had been observed with the ligands previously discussed, even though **4** would have a formal charge of +1 under the assay conditions (Table 2). Further examination of the residues of the CDK4M2 construct revealed that not all of the variations between the two CDK isoforms, particularly the Q131E exchange, had been accounted for in this mimic protein. To examine the effects of the $E144^{CDK4}$ residue present in place of Q131 in CDK2, the latter was replaced with a Glu residue in the context of the mimic protein and the interaction energies were recalculated. The results showed that the nonbonded energies were now considerably more favorable, the total increasing from −32 to −54 kcal/mol, mainly due to the Coulombic contribution. This result confirms that $E144^{CDK4}$ provides a considerable proportion of the binding free energy for CDK4 inhibitors and that interaction with this residue should be accounted for in the design of compounds that are selective for this kinase. Activity testing of the CDK4M2 protein did indeed show that the inhibitors were about 10-fold less potent on the CDK4 mimic than against the native CDK4/cyclin D1 complex. These results suggest that this potency difference could be reduced by incorporation of the Q131E mutation into the mimic protein and that this construct would give a more accurate representation of the native CDK4 binding mode.

As an additional validation of the CDK4 homology structure generated for our present study, the nonselective compound **5** (Table 2) was docked into CDK4 and the resulting binding mode compared with that found in the CDK4M2 crystal structure complex. It was found that very close overlays were obtained between the pose observed in the CDK4M2 and those for the inhibitor in complex with the model structure. In addition, calculation of the nonbonded energies in each case (CDK2,

CDK4M2, and CDK4 model complexes) showed that these were comparable and therefore consistent with the similar IC_{50}'s for this inhibitor against both CDK2 and CDK4. This result provides additional validation that a general correlation of this nature can be made and that the CDK4 model structure provides a structural rationale for CDK4 selectivity.

To provide further conformation of the CDK4 selectivity hypothesis, the pK_a value was calculated for the ionizable N of the CDK inhibitor flavopiridol (Table 2, **6**), which preferentially inhibits CDK4 over CDK2 (3- to 5-fold) [26]. The resulting value of 8.5 again demonstrates that this feature contributes to the selectivity profile of CDK4 inhibitors.

Design of CDK4-Selective Compounds Based on the 2-anilino-4-(thiazol-5-yl)pyrimidine System

We have shown recently that potent and selective ATP-competitive CDK inhibitor compounds can be generated from the 2-anilino-4-(thiazol-5-yl)pyrimidine template [22, 24]. In our hands, this pharmacophore to date has yielded predominantly CDK2-selective inhibitors, some of them with nanomolar or subnanomolar potency. Furthermore, we have crystallized several analogs in complex with CDK2 and therefore have a good understanding of the structure-activity relationship of the pharmacophore with respect to CDK2. The main determinants for high-potency binding include the H bond donor/acceptor pair involving the bridging anilino NH and the pyrimidine N6 to the hinge region of CDK2; a nonpolar contact from the thiazol-4-yl methyl group with F80, H bonding contacts from polar thiazole substituents with Q131, and van der Waals and H bonds from the pyrimidine and aniline aromatic rings (V18, D86, K89, and L134). The aniline ring is in the position corresponding to the charged group determined in this study to contribute to CDK4 selectivity. In order to probe the identified CDK4 selectivity determinants in the context of the aminopyrimidine system, compounds that incorporated ionizable groups on the anilino ring were designed and synthesized. Table 3 shows the structures of several compounds incorporating anilines substituted with amine, methylamine, morpholine, and various piperazines. In addition, the pK_as for the primary ionizable groups in these substituents was calculated. As negative controls, potential inhibitors incorporating a morpholine ring (**5**) (isosteric with piperazine) and an acetylated primary amino group (**3**) were synthesized. Neither of these compounds has a substituent capable of forming ion-pair interactions with $E144^{CDK4}$ (nonconserved with CDK2) and $D99^{CDK4}$ (conserved with CDK2). Furthermore, the benzenediamine compound **4**, whose aniline NH_2 function is positively charged only below pH 5, was analyzed. Testing of the compounds in Table 3 in both CDK2/E and CDK4/D1 kinase assays revealed that only the compounds with a function associated with the aniline ring that is protonated at pH 7 exhibited selectivity for CDK4. In contrast, all of the inhibitors without this characteristic were partially selective for CDK2. In particular, comparison of compounds **5** and **6**, which differ only by the oxygen-to-nitrogen replacement in the saturated ring, demonstrates that the piperazine inhibitor has a more than 20-fold enhancement in CDK4 activity, while its CDK2 inhibition is increased by only 2-fold. Of the selective inhibitors, compound **10**, which contains a piperazine ring, was the most selective with a 30-fold higher potency in the CDK4/D1 kinase assay. Inhibitors containing methylpiperazine (**7**) and hydroxyethylpiperazine (**8**) also exhibited CDK4 selectivity; however, they did so to a lesser degree.

Structural Basis for CDK4 Selectivity of Anilinopyrimidines

To date, several hundred compounds in the anilinopyrimidine series have been synthesized; analogs **1, 2, 6, 7, 8,** and **10**, however, are the first examples of CDK4-selective derivatives in this series. The observed preferential binding of these compounds to CDK4 thus confirmed the initial design hypothesis that appropriate introduction of positively charged groups into the inhibitor results in increased CDK4 selectivity. As a further test of the hypothesis, the pK_a values for the ionizable nitrogens in each of the inhibitors were calculated (Table 3). As can be seen from this table, all the CDK4-selective compounds have a pK_a of seven or greater and, thus, would be partially or fully charged at the pH conditions in which the assay was performed. There is no correlation, however, between the basisity of the nitrogen and the extent of observed selectivity for CDK4, therefore suggesting that other determinants contribute to the selectivity. In order to determine all of the factors contributing to binding of these compounds to both CDK2 and CDK4, docking with the homology structure and modeling calculations in the context of the available CDK2-complex crystal structures were carried out with compounds **1, 5, 6,** and **10**. For inhibitor **1**, containing a meta-aminomethyl group on the aniline ring, the docked structure showed that it forms the expected binding mode with CDK4 and has similar interaction energies to those observed for other potent CDK4 inhibitors. Modeling of the aminomethyl interactions for compound **1** with CDK2 indicates that much less favorable interaction energies are obtained compared to CDK4, resulting from Coulombic and van der Waals repulsion with $K89^{CDK2}$. Comparison of the binding of inhibitors **5** and **6** to the ATP site of both enzymes is significant in this case, given that they only differ by the NH of the piperazine ring (morpholine in **5**) and is significant given that **6** is selective for CDK4 (Table 3). Energetic analysis suggests as before that the positively charged NH group of the piperazine ring contributes extensively to CDK4 binding through interaction with $E144^{CDK4}$ and $D99^{CDK4}$ and, thus, is consistent with the selectivity hypothesis. The highly CDK4 selective inhibitor **10**, having an IC_{50} of 7 nM against CDK4/D1, was docked into the ATP binding site of CDK4. The resulting binding mode very closely represents the structure observed with **6** and overlay of the inhibitor with the crystallographically derived CDK2 complex of **9** (Figure 4) indicates the electrostatic interaction with $E144^{CDK4}$ results in the piperazine ring moving significantly toward the acidic residues. As can be seen, the intermolecular contacts of thiazole and pyrimidine rings match closely in both cases; however, interactions of the saturated ring result in its displacement (and that of the aniline) with respect to the position of the corresponding rings of **9** in the CDK2 active site. Overall,

Table 3. In Vitro Potencies, pK_a, and Selectivity Ratios for Aminopyrimidine Compounds

Structure

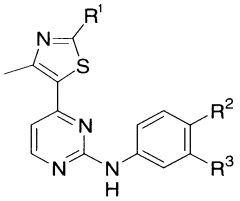

Number	R^1	R^2	R^3	pK_a	Kinase Inhibition (μm) CDK4/D1	CDK2/E	CDK4 Selectivity (Fold)
1	NHMe	H	CH_2NH_2	9.6	0.23	0.41	1.8
2	NHEt	H	CH_2NH_2	9.6	0.11	0.33	3.0
3	NHMe	H	CH_2NHAc	–	0.89	0.43	0.5
4	Me	NH_2	H	4.0	3.8	0.23	0.1
5	Me		H	3.7	4.0	2.0	0.5
6	Me		H	9.0	0.64	1.1	1.7
7	Me		H	7.3	0.16	1.02	6.4
8	Me	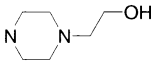	H	7.4	0.43	2.2	5.1
9	NH_2		H	3.7	2.40	1.0	0.4
10	NHMe		H	9.0	0.007	0.22	31.4

inhibitor **10** exhibits striking complementarity with the ATP cleft and very favorable nonbonded energetics, in line with the in vitro potency of this compound. The structure also presents evidence for the increase in potency of this compound relative to **6**, which only differs in the thiazole substitution. The methylamino group on the thiazole ring of **10** contributes hydrogen bonds to $E158^{CDK4}$ and the piperazine ring additionally provides vdW surface complementarity with the specificity surface. These interactions most likely provide the majority of the increase in affinity of this ligand. Analysis of the nonbonded energies for both compounds again correlates well with in vitro potency.

The docking experiments also provide insight into the potency and selectivity of compounds **7** and **8**, having methyl- and hydroxyethyl-substituted piperazines, respectively. These two inhibitors have a less-basic piperazinyl nitrogen and, hence, would be expected to be less selective for CDK4; however, the converse is true. The results suggest that the piperazine substituents provide an increase in potency through vdW contacts with the Cγ of $R101^{CDK4}$. As discussed previously, the increased selectivity of **7** and **8** is likely due to the steric consequence of the additional group adjacent to $K89^{CDK2}$, resulting in lower affinity for CDK2. The methylated (**7**) and hydroxyethyl (**8**) piperazines would therefore bind less potently to CDK2 and be more selective for CDK4. The additional space provided by $T102^{CDK4}$, in comparison to $K89^{CDK2}$, thus would enable these inhibitors to bind with higher affinity to CDK4.

Very recent publications have detailed a pharmacophore that has common structural features with the novel CDK4 selective compounds we have described [15, 27]. This series of inhibitors contains a pyrimidine derivatized with two aniline groups (Table 2, **7**). All of the compounds described contain a hydroxy-dimethylaminopropane function that has a calculated pK_a of 8.7. In the deposited CDK2-complex structures, the position of the charged group is directly analogous to that observed for the substituted piperazine groups in the inhibitors disclosed here. Several analogs are reported that have varying levels of inhibition against CDK2 and CDK4. The structure of these inhibitors is consistent with the selectivity hypothesis proposed here, since all of the compounds contain the same protonated group and are between 5- and 20-fold selective for CDK4. Interestingly, the compounds that are optimized for CDK4 binding also undergo a similar relative increase in CDK2 activity. This suggests that for these examples, the charged functional group contributes extensively to the observed selectivity, and additional interactions with residues common to both kinases result in the increase in binding to both CDKs.

Significance

We have performed an in-depth computational investigation into the pharmacophoric requirements for selective inhibition of CDK4. The results obtained demonstrate that two major determinants of CDK4-

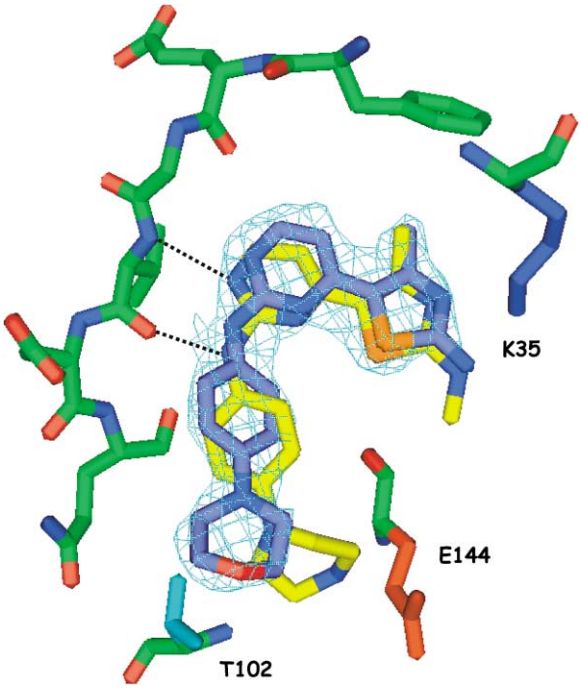

Figure 4. Comparison of Ligand Positions of Compounds **10** and **9**

For **9** (blue carbons, CDK2), the X-ray structure in complex with CDK2/cyclin A was used, while for **10** (yellow carbons, CDK4), the bound structure was predicted by affinity docking with CDK4. Electron density for inhibitor **10** is displayed in light blue. The similarity on the pyrimidine and thiazole functions is apparent in the two structures, while interactions of the piperazine with E144 results in significant movement and displacement of this ring in conjunction with the aniline.

specific binding are as follows. (1) There is a requirement for the geometrically appropriate presence of a function in the inhibitor that is positively charged at physiological pH. This functionality results in a more favorable Coulombic energy of interaction between the ATP cleft of CDK4 (D99^{CDK4}, E144^{CDK4}) and repulses the inhibitor from the active site of CDK2 through K89^{CDK2}. (2) The incorporation of a bulky substituent in the inhibitor that occupies the volume of the ATP site proximal to K89^{CDK2} and D86^{CDK2}. This group precludes effective binding to CDK2 through steric hindrance with these residues and, in some cases, results in disruption of effective H bonds to the hinge region of the kinase.

The suitable incorporation of these determinants into a known CDK2-selective molecule or into a nonoptimal CDK4 inhibitor should facilitate the development of an inhibitor that binds with higher affinity and preferentially to CDK4/cyclin D1, or alternatively, these features could be used to modify nonselective low-affinity lead compounds to interact more favorably with this complex.

Experimental Procedures

Homology Model Construction

The homology model for CDK4 was generated by using the program module Homology within the molecular modeling package InsightII (Accelrys, San Diego, CA). For the model construction, the CDK2 (1CKP, resolution 2.0 Å) and CDK6 (1BLX, resolution 1.9 Å) structures were used. Sequence alignment of CDK4 with CDK2 was performed by using the PAM 120 multiple scoring matrix with a dimension block of 0.6, a high significance p value of 0.0001, a not significant p value of 0.1 and a pairwise threshold of 60. By using a combination of the two structures to generate coordinates for the regions that had the highest identity in each kinase, a model structure for the kinase domain was constructed. The strategy generally involved using CDK2 to define the structurally conserved regions (SCRs) from which the coordinates were subsequently transferred. This was followed by loop construction where the non-SCRs were generated from CDK2 and CDK6 and additionally by de novo building and subsequent evaluation of the most realistic coordinates (in terms of energetics of the loops and the exclusion of loops leading to overlapping atoms). After loop building was completed for missing coordinates, the raw coordinates were refined by using successive rounds of end repair splice repairing with an omega force constant of 50 and energy minimization (100 steps of steepest descent to a derivative of 5). The model was then completed through a further minimization and 1 ps of molecular dynamics to explore more fully the conformational space of the loop regions. The final model structure was checked against databases of protein structures for bond length and dihedral angle violations. The results indicated that these as a whole were within acceptable limits with >80% of residues having phi-psi plots within the allowed region in Ramachandran space.

Molecular Modeling

The structure coordinates of the ternary complex of CDK2/cyclin A/p27^{KIP1} were obtained from the RCSB (accession code 1JSU). CDK inhibitors were docked into the ATP site of the CDK2 X-ray crystal structure or the CDK4 model structure by using the Affinity program (Molecular Simulations, San Diego, CA). The binding site was defined as an 8 Å radius from the center of a ligand binding mode. This molecular docking routine, which incorporates a full molecular mechanics approach, allows for flexibility both in the ligand and in the side chains and backbone of the receptor (the positions of the α carbon atoms were fixed during the simulation). The calculation was performed by using the CVFF force field in a two-step process with an implicitly derived solvation model and geometric H bond restraints. For the initial phase of the calculation, the inhibitor was minimized into the ATP cleft by using a simple, nonbonded method where the Coulombic and van der Waals terms are scaled to zero and 0.1, respectively. The subsequent refinement phase involved conformational sampling by using molecular dynamics calculated over 5 ps in 100 fs stages, where the temperature was scaled from 500 to 300 K. The calculation was completed by a final minimization over 1000 steps using the Polak-Ribiere conjugate gradient method. The docked structures were ranked energetically (by using the in house developed programs Calsor and Calsorcont, values reported in kcal/mol) and by consistency of the nonbonded contacts with known CDK and kinase interactions in order to determine the most representative binding mode. While the values obtained for intermolecular interaction energies obtained using Affinity are not completely accurate, they have been found in this study and in others to correlate with inhibitor potency when compared within a chemical series. The absolute values should not necessarily be considered to reflect the actual binding constant.

pK_a Calculation

pK_a values of the ionizable nitrogens for the CDK inhibitors were calculated by using the ACD Labs (Toronto, Canada) pK_a DB software. ACD pK_a DB is a program that calculates accurate acid-base ionization constants (pK_a values) at 25°C and zero ionic strength in aqueous solutions and is reported to have a general accuracy of $\pm$0.2 pK_a units.

Assay Screening, Protein Expression, and X-Ray Crystallography

Kinase assays were performed according to the previously published procedure [22]. Protein expression, purification, and crystallography were carried out as outlined [28].

Synthesis of Aminopyrimidine Analogs

A Typical Procedure for Preparation of 3-dimethylamino-1-(thiazol-5-yl)propenone

A solution of 3-chloropentane-2,4-dione (2.5 g, 19 mmol) in MeOH (10 mL) was treated with methyl thiourea (1.67 g, 19 mmol) and pyridine (1.5 mL). The mixture was stirred at room temperature for 2 hr. Precipitated 1-(4-methyl-2-methylaminothiazol-5-yl)ethanone (2.10 g, 65%) was filtered, washed with Et_2O, and dried. Mp 201°C–203°C. Anal. RP-HPLC (Vydac 218TP54 250 × 4.6 mm column; linear gradient elution using H_2O/MeCN containing 0.1% CF_3COOH): t_R 5.5 min (10%–70% MeCN, purity 100%). ^{1}H-NMR (500 MHz, $CDCl_3$): δ 2.47 (s, 3H, CH_3), 2.61 (s, 3H, CH_3), 3.18 (s, 3H, CH_3). ^{13}C-NMR (DMSO-d_6): δ 19.16, 30.05, 31.54, 49.28, 121.78, 158.54, 188.81. MS (ESI^+) *m/z* 170.87 ($C_7H_{10}N_2OS$ requires 170.23). This material (2.05 g, 12 mmol) was suspended in *N,N*-dimethylformamide dimethylacetal (5.3 mL, 4.80 g, 40 mmol), and the mixture was heated at 120°C with stirring for 16 hr. After cooling, the reaction mixture was evaporated to dryness. The residue was crystallized from EtOAc to afford 3-dimethylamino-1-(4-methyl-2-methylaminothiazol-5-yl)propenone as an orange solid (1.82 g, 67%): mp 209°C–211°C. Anal. RP-HPLC: t_R 7.1 min (10%–70% MeCN, purity 100%). ^{1}H-NMR ($CDCl_3$): δ 2.55 (s, 3H, CH_3), 2.94 (s, 3H, CH_3), 3.41 (s, 6H, CH_3), 5.30 (d, 1H, *J* = 12.2 Hz, CH), 7.64 (d, 1H, *J* = 12.2 Hz, CH). ^{13}C-NMR (DMSO-d_6): δ 18.94, 31.41, 54.99, 94.32, 122.05, 152.96, 153.83, 169.41, 179.89. MS (ESI^+) *m/z* 226.11 (M+H]). Anal. ($C_{10}H_{15}N_3OS$.MeOH) C, H, N.

3-Dimethylamino-1-(2-ethylamino-4-methylthiazol-5-yl)propenone

Mp 204°C–205°C. Anal. RP-HPLC: t_R 7.3 min (10%–70% MeCN, purity 100%). ^{1}H-NMR ($CDCl_3$): δ 1.25 (t, 3H, *J* = 6.0 Hz, CH_3), 2.49 (s, 3H, CH_3), 3.20 (s, 6H, CH_3), 3.28 (m, 2H, CH_2), 5.35 (d, 1H, *J* = 11.5 Hz, CH), 7.67 (d, 1H, *J* = 11.5 Hz, CH). ^{13}C-NMR (DMSO-d_6): δ 14.92, 18.95, 31.41, 54.99, 94.34, 121.81, 152.92, 153.74, 168.49, 179.90. MS (ESI^+) *m/z* 240.17 $(M+H)^+$($C_{11}H_{17}N_3OS$ requires 239.34).

3-Dimethylamino-1-(2,4-dimethylthiazol-5-yl)propenone

Mp 96°C–98°C. Anal. RP-HPLC: t_R 7.1 min (10%–70% MeCN, purity 100%). ^{1}H-NMR ($CDCl_3$): δ 2.66 (s, 6H, CH_3), 2.70 (s, 6H, CH_3), 5.37 (d, 1H, *J* = 12.2 Hz, CH), 7.66 (d, 1H, *J* = 12.2 Hz, CH). ^{13}C-NMR (DMSO-d_6): δ 18.19, 19.52, 37.77, 45.19, 94.50, 134.01, 153.62, 154.38, 165.64, 179.93. MS (ESI^+) *m/z* 211.01 $(M+H)^+$. Anal. ($C_{10}H_{14}N_2OS$) C, H, N.

General Procedure for Paration of N-phenyl-guanidine Nitrates

To an ice-cooled mixture of the appropriate aniline (25 mmol) in EtOH (6 mL) nitric acid (1.8 ml of 70% solution in H_2O) was added dropwise with stirring. After complete addition, cyanamide (5 ml of 50% solution in H_2O) was added, and the mixture was heated at 100°C for 16–18 hr under N_2. After cooling to room temperature, it was poured into excess Et_2O and was basified with aq NaOH solution. The ethereal layer was separated, and the aqueous phase was extracted with Et_2O several times. The combined organic phases were washed with brine, dried on $MgSO_4$, filtered, and evaporated. The resulting residue was purified by crystallization or flash chromatography in appropriate mixtures of EtOAc/PE or EtOAc/MeOH.

General Procedure for Preparation of [4-(thiazol-5-yl)pyrimidin-2-yl]phenylamines

A mixture of 3-dimethylamino-1-(thiazol-5-yl)propenone (1 equiv), the appropriate N-phenyl-guanidine nitrate (2 equiv), and NaOH (1 equiv) in 2-methoxyethanol were heated at 125°C for 22 hr under N_2. After cooling, the solvent was evaporated, and the residue was purified by flash chromatography with appropriate mixtures of EtOAc/hexane as the eluant. Pure products were obtained following recrystallization.

3-[4-(2-Methylamino-4-methyl-thiazol-5-yl)pyrimidin-2-yl-amino-benzylacetamide (1)

Mp. 253°C–255°C. Anal. RP-HPLC: t_R = 11.3 min (10%–70% MeCN, purity >95%): ^{1}H NMR (DMSO-D_6): δ 1.86 (s, 3H, CH_3), 2.46 (s, 3H, CH_3), 2.85 (s, 2H, CH_2), 3.09 (s, 3H, CH_3), 6.82 (d, 1H, *J* = 8.0 Hz, ph-H), 6.88 (d, 1H, *J* = 5.5 Hz, pyrimidinyl-H), 7.2 (t, 1H, *J* = 8.0 Hz, Ph-H), 7.60 (d, 1H, *J* = 8.0 Hz, Ph-H), 7.73 (s, 1H, Ph-H), and 8.32 (d, 1H, *J* = 5.5 Hz, pyrimidinyl-H). MS (ESI^+) m/z 391.55 [M+Na] ($C_{18}H_{20}N_6OSNa$ requires 391.46).

3-[4-(2-Ethylamino-4-methyl-thiazol-5-yl)pyrimidin-2-yl-amino]benzylamine (2)

Mp. 290°C–292°C. Anal. RP-HPLC: t_R = 10.6 min (10%–70% MeCN, purity >95%). ^{1}H-NMR (DMSO-D_6) δ: 1.31 (t, 3H, *J* = 7.0 Hz, CH_3), 2.64 (s, 3H, CH_3), 3.54 (m, 2H, CH_2), 4.11 (m, 2H, CH_2), 7.14 (d, 1H, *J* = 6.0 Hz, pyrimidinyl-H), 7.22 (d, 1H, *J* = 8.0 Hz, Ph-H), 7.45 (t, 1H, *J* = 8.0 Hz, Ph-H), 7.74 (d, 1H, *J* = 8.0 Hz, Ph-H), 7.95 (s, 1H, Ph-H), 8.53 (d, 1H, *J* = 6.0 Hz, pyrimidinyl-H). MS (ESI^+) m/z 341.20 $[M+H]^+$ ($C_{17}H_{20}N_6S$ requires 340.45).

3-[4-(2-Ethylamino-4-methyl-thiazol-5-yl)pyrimidin-2-yl-amino]benzylacetamide (3)

Anal. RP-HPLC: t_R = 12.7 min (0%–60% MeCN, purity >95%). ^{1}H-NMR (CD_3OD) δ: 1.17 (t, 3H, *J* = 7.5 Hz, CH_3), 1.98 (s, 3H, CH_3), 2.51 (s, 3H, CH_3), 3.36 (q, 2H, *J* = 7.1 Hz, CH_2), 4.39 (s, 2H, CH_2), 6.92 (m, 2H, pyrimidinyl-H and Ph-H), 7.25 (t, 1H, *J* = 7.6 Hz, Ph-H), 7.49 (m, 1H, Ph-H), 7.79 (sbr, 1H, Ph-H), 8.25 (d, 1H, *J* = 5.5 Hz, pyrimidinyl-H). MS (ESI^+) m/z 383.46 $[M+H]^+$ ($C_{19}H_{22}N_6OS$ requires 382.48).

N-[4-(2,4-Dimethyl-thiazol-5-yl)pyrimidin-2-yl]-benzene-1,4-diamine (4)

Mp. 206°C–208°C. ^{1}H-NMR (DMSO-D_6) δ: 2.59 (s, 3H, CH_3), 2.62 (s, 3H, CH_3), 4.75 (brs, 2H, NH_2), 6.51 (d, 2H, *J* = 7.8Hz, Ph-H), 6.91 (d, 1H, *J* = 4.9Hz, pyrimidinyl-H), 7.31 (d, 2H, *J* = 7.8Hz, Ph-H), 8.38 (d, 1H, *J* = 5.4Hz, pyrimidinyl-H), 9.11 (s, 1H, NH). MS (ESI^+) m/z 298.03 $[M+H]^+$ ($C_{15}H_{15}N_5S$ requires 297.38).

[4-(2,4-Dimethyl-thiazol-5-yl)pyrimidin-2-yl](4-morpholin-4-yl-phenyl)amine (5)

Mp. 280°C–282°C. ^{1}H-NMR ($CDCl_3$) δ: 2.69 (s, 3H, CH_3), 2.70 (s, 3H, CH_3), 3.14 (t, 4H, *J* = 4.8 Hz, CH_2), 3.72 (t, 4H, *J* = 4.9 Hz, CH_2), 6.89 (d, 1H, *J* = 5.1 Hz, pyrimidinyl-H), 6.95 (d, 2H, *J* = 8.8 Hz, Ph-H), 6.98(br. s, 1H, NH), 7.53 (d, 2H, *J* = 9.1 Hz, Ph-H), 8.38 (d, 1H, *J* = 5.1 Hz, pyrimidinyl-H). MS (ESI^+) m/z 368.01 $[M+H]^+$ ($C_{19}H_{21}N_5OS$ requires 367.47).

[4-(2,4-Dimethyl-thiazol-5-yl)pyrimidin-2-yl](4-piperazin-1-yl-phenyl)amine (6)

Mp. 301°C–303°C. ^{1}H-NMR ($CDCl_3$) δ: 2.62 (s, 3H, CH_3), 2.63 (s, 3H, CH_3), 2.99 (m, 4H, CH_2), 3.06 (m, 4H, CH_2), 6.81 (d, 1H, *J* = 5.4 Hz, pyrimidinyl-H), 6.89 (m, 3H, Ph-H, NH), 7.44 (m, 2H, Ph-H), 8.31 (d, 1H, *J* = 5.4 Hz, pyrimidinyl-H). MS (ESI^+) m/z 367.20 $[M+H]^+$ ($C_{19}H_{22}N_6S$ requires 366.48).

[4-(2,4-Dimethyl-thiazol-5-yl)pyrimidin-2-yl][4-(4-methyl-piperazin-1-yl)phenyl]amine (7)

^{1}H-NMR ($CDCl_3$) δ: 2.37 (s, 3H, CH_3), 2.61 (m, 4H, CH_2), 2.69 (s, 3H, CH_3), 2.70 (s, 3H, CH_3), 3.20 (m, 4H, CH_2), 6.88 (d, 1H, *J* = 5.1 Hz, pyrimidinyl-H), 6.94 (s, 1H, NH), 6.96 (d, 2H, *J* = 8.8 Hz, Ph-H), 7.51 (d, 2H, *J* = 8.8 Hz, Ph-H), 8.38 (d, 1H, *J* = 5.1 Hz, pyrimidinyl-H).

2-(4-{4-[4-(2,4-Dimethyl-thiazol-5-yl)pyrimidin-2-ylamino]phenyl}piperazin-1-yl)ethanol (8)

^{1}H-NMR ($CDCl_3$) δ: 2.55 (t, 2H, *J* = 5.4 Hz, CH_2), 2.62 (m, 10H, CH_3 & CH_2), 3.12 (t, 4H, *J* = 4.9 Hz, CH_2), 3.60 (t, 2H, *J* = 5.4 Hz, CH_2), 6.81 (d, 1H, *J* = 5.4 Hz, pyrimidinyl-H), 6.88 (m, 2H, Ph-H), 7.05 (br. s, 1H, NH), 7.45 (m, 2H, Ph-H), 8.30 (d, 1H, *J* = 5.1 Hz, pyrimidinyl-H). MS (ESI^+) m/z 411.70 $[M+H]^+$ ($C_{21}H_{26}N_6OS$ requires 410.54).

[4-(2-Amino-4-methyl-thiazol-5-yl)-pyrimidin-2-yl]-(4-morpholin-4-yl-phenyl)-amine [9]

Mp. 300°C–304°C: ^{1}H-NMR (DMSO-d_6) δ: 2.46 (s, 3H, CH_3), 3.07 (m, 4H, CH_2), 3.76 (m, 4H, CH_2), 6.85 (d, 1H, *J* = 5.3 Hz, pyrimidinyl-H), 6.92 (m, 2H, Ph-H), 7.53 (br. s, 1H, NH), 7.67 (m, 2H, Ph-H), 8.30 (d, 1H, *J* = 5.4 Hz, pyrimidinyl-H), 9.25 (br. s, 1H, NH). MS (ESI^+) m/z 369 $[M+H]^+$ ($C_{18}H_{20}N_6OS$ requires 368.5).

[4-(2-Methylamino-4-methyl-thiazol-5-yl)pyrimidin-2-yl](4-piperazin-1-yl-phenyl)amine (10)

Anal. RP-HPLC: t_R = 8.8 min (10%–70% MeCN, purity >95%). ^{1}H-NMR (DMSO-d_6) δ: 2.45 (3, 3H, CH_3), 2.83 (t, 4H, *J* = 5.9Hz, CH_2), 2.85 (d, 3H, *J* = 4.9Hz, CH_2), 2.95 (t, 4H, *J* = 4.9Hz, CH_2), 6.81 (d, 1H, *J* = 5.4Hz, pyrimidinyl-H), 6.85 (d, 2H, *J* = 9.3Hz, Ph-H), 7.58 (d, 2H, *J* = 8.8Hz, Ph-H), 7.99 (m, 1H, NH), 8.26 (d, 1H, *J* = 5.4Hz, pyrimidinyl-H), 9.14 (brs, 1H). MS (ESI^+) m/z 382.06 $[M+H]^+$ ($C_{19}H_{23}N_7S$ requires 381.50).

Acknowledgments

The authors would like to thank Brian McClue and Richard Main for IT support, and Professor Malcolm Walkinshaw (University of Edinburgh) and Dr. Howard Marriage (Cyclacel) for helpful discussions and proof reading of this manuscript.

Received: November 28, 2003
Revised: January 15, 2004
Accepted: January 21, 2004
Published: April 16, 2004

References

1. Morgan, D. (1997). Cyclin-dependent kinases: engines, clocks, and microprocessors. Annu. Rev. Cell Dev. Biol. *13*, 261–291.
2. Morgan, D., Fisher, R.P., Espinoza, F.H., Farrell, A., Nourse, J., Chamberlin, H., and Jin, P. (1998). Control of eukaryotic cell cycle progression by phosphorylation of cyclin-dependent kinases. Cancer J. Sci. Am. Suppl. *1*, S77–S83.
3. Sherr, C.J. (1996). Cancer cell cycles. Science *274*, 1672–1677.
4. Chen, Y.-N.P., Sharma, S.K., Ramsey, T.M., Jiang, L., Martin, M.S., Baker, K., Adams, P.D., Bair, K.W., and Kaelin, W.G. (1999). Selective killing of transformed cells by cyclin/cyclin-dependent kinase 2 antagonists. Proc. Natl. Acad. Sci. USA *96*, 4325–4329.
5. McInnes, C., Andrews, M.J., Zheleva, D.I., Lane, D.P., and Fischer, P.M. (2003). Peptidomimetic design of CDK inhibitors targeting the recruitment site of the cyclin subunit. Curr. Med. Chem. Anti-Canc. Agents *3*, 57–69.
6. Garcia-Echeverria, C., Traxler, P., and Evans, D.B. (2000). ATP site-directed competitive and irreversible inhibitors of protein kinases. Med. Res. Rev. *20*, 28–57.
7. Fischer, P.M., Endicott, J., and Meijer, L. (2003). Cyclin-dependent kinase inhibitors. In Progress in Cell Cycle Research, Volume *5*, L. Meijer, A. Jézéquel, and M. Roberge, eds. (Roscoff, France: Editions de la Station Biologique de Roscoff), pp. 235–248.
8. Fischer, P.M. (2001). Recent advances and new directions in the discovery and development of cyclin-dependent kinase inhibitors. Curr. Opin. Drug Discov. Dev. *4*, 623–634.
9. Senderowicz, A.M. (2003). Small-molecule cyclin-dependent kinase modulators. Oncogene *22*, 6609–6620.
10. Ortega, S., Malumbres, M., and Barbacid, M. (2002). Cell cycle and cancer: the G1 restriction point and the G1/S transition. Curr. Genomics *3*, 245–263.
11. Harbour, J.W., Luo, R.X., Dei Santi, A., Postigo, A.A., and Dean, D.C. (1999). Cdk phosphorylation triggers sequential intramolecular interactions that progressively block Rb functions as cells move through G1. Cell *98*, 859–869.
12. Harbour, J.W., and Dean, D.C. (2000). The Rb/E2F pathway: expanding roles and emerging paradigms. Genes Dev. *14*, 2393–2409.
13. Lees, J.A., and Weinberg, R.A. (1999). Tossing monkey wrenches into the clock: new ways of treating cancer. Proc. Natl. Acad. Sci. USA *96*, 4221–4223.
14. Barvian, M., Boschelli, D.H., Crossrow, J., Dobrusin, E., Fattaey, A., Fritsch, A., Fry, D., Harvey, P., Keller, P., Garrett, M., et al. (2000). Pyrido[2,3-d]pyrimidin-7-one inhibitors of cyclin-dependent kinases. J. Med. Chem. *43*, 4606–4616.
15. Beattie, J.F., Breault, G.A., Ellston, R.P.A., Green, S., Jewsbury, P.J., Midgley, C.J., Naven, R.T., Minshull, C.A., Pauptit, R.A., Tucker, J.A., et al. (2003). Cyclin-dependent kinase 4 inhibitors as a treatment for cancer. Part 1: identification and optimisation of substituted 4,6-Bis anilino pyrimidines. Bioorg. Med. Chem. Lett. *13*, 2955–2960.
16. Carini, D.J., Kaltenbach, R.F., Liu, J., Benfield, P.A., Boylan, J., Boisclair, M., Brizuela, L., Burton, C.R., Cox, S., Grafstrom, R., et al. (2001). Identification of selective inhibitors of cyclin dependent kinase 4. Bioorg. Med. Chem. Lett. *11*, 2209–2211.
17. Honma, T., Hayashi, K., Aoyama, T., Hashimoto, N., Machida, T., Fukasawa, K., Iwama, T., Ikeura, C., Ikuta, M., Suzuki-Takahashi, I., et al. (2001). Structure-based generation of a new class of potent Cdk4 inhibitors: new de novo design strategy and library design. J. Med. Chem. *44*, 4615–4627.
18. Honma, T., Yoshizumi, T., Hashimoto, N., Hayashi, K., Kawanishi, N., Fukasawa, K., Takaki, T., Ikeura, C., Ikuta, M., Suzuki-Takahashi, I., et al. (2001). A novel approach for the development of selective Cdk4 inhibitors: library design based on locations of Cdk4 specific amino acid residues. J. Med. Chem. *44*, 4628–4640.
19. Kubo, A., Kazuhiko, N., Varma, R.K., Conrad, N.K., Cheng, J.Q., Lee, W.-C., Testa, J.R., Johnson, B.E., Kaye, F.J., and Kelley, M.J. (1999). The p16 status of tumor cell lines identifies small molecule inhibitors specific for cyclin-dependent kinase 4′. Clin. Cancer Res. *5*, 4279–4286.
20. Soni, R., Muller, L., Furet, P., Schoepfer, J., Stephan, C., Zumstein-Mecker, S., Fretz, H., and Chaudhuri.B. (2000). Inhibition of cyclin-dependent kinase 4 (Cdk4) by fascaplysin, a marine natural product. Biochem. Biophys. Res. Commun. *275*, 877–884.
21. Nugiel, D.A., Vidwans, A., Etzkorn, A.M., Rossi, K.A., Benfield, P.A., Burton, C.R., Cox, S., Doleniak, D., and Seitz, S.P. (2002). Synthesis and evaluation of indenopyrazoles as cyclin-dependent kinase inhibitors. 2. Probing the indeno ring substituent pattern. J. Med. Chem. *45*, 5224–5232.
22. Wu, S.Y., McNae, I., Kontopidis, G., McClue, S.J., McInnes, C., Stewart, K.J., Wang, S., Zheleva, D.I., Marriage, H., Lane, D.P., et al. (2003). Discovery of a novel family of CDK inhibitors with the program LIDAEUS: structural basis for ligand-induced disordering of the activation loop. Structure *11*, 399–410.
23. Ikuta, M., Kamata, K., Fukasawa, K., Honma, T., Machida, T., Hirai, H., Suzuki-Takahashi, I., Hayama, T., and Nishimura, S. (2001). Crystallographic approach to identification of cyclin-dependent kinase 4 (CDK4)-specific inhibitors by using CDK4 mimic CDK2 protein. J. Biol. Chem. *276*, 27548–27554.
24. Wang, S.C.M. Wood, G., Osnowski, A., Anderson, S., Yuill, R., Thomas, M., Jackson, W., Midgley, C., Griffiths, G., McNae, I., et al. (2004). 2-Anilino-4-(Thiazol-5-yl)Pyrimidine CDK inhibitors: synthesis, SAR analysis, X-ray crystallograghy, and biological activity. J. Med. Chem. *47*, 1662–1675.
25. Fry, D.W., Bedford, D.C., Harvey, P.H., Fritsch, A., Keller, P.R., Wu, Z., Dobrusin, E., Leopold, W.R., Fattaey, A., and Garrett, M.D. (2001). Cell cycle and biochemical effects of PD 0183812. A potent inhibitor of the cyclin D-dependent kinases CDK4 and CDK6. J. Biol. Chem. *276*, 16617–16623.
26. Carlson, B.A., Dubay, M.M., Sausville, E.A., Brizuela, L., and Worland, P.J. (1996). Flavopiridol induces G1 arrest with inhibition of cyclin-dependent kinase (CDK) 2 and CDK4 in human breast carcinoma cells. Cancer Res. *56*, 2973–2978.
27. Breault, G.A., Ellston, R.P., Green, S., James, S.R., Jewsbury, P.J., Midgley, C.J., Pauptit, R.A., Minshull, C.A., Tucker, J.A., and Pease, J.E. (2003). Cyclin-dependent kinase 4 inhibitors as a treatment for cancer. Part 2: identification and optimisation of substituted 2,4-bis anilino pyrimidines. Bioorg. Med. Chem. Lett. *13*, 2961–2966.
28. Kontopidis, G., Andrews, M.J.I., McInnes, C., Cowan, A., Powers, H., Innes, L., Plater, A., Griffiths, G., Paterson, D., Zheleva, D.I., et al. (2003). Insights into cyclin groove recognition: complex crystal structures and inhibitor design through ligand exchange. Structure *11*, 1537–1546.
29. DeLano, W.L. (2002). The PyMOL Molecular Graphics System (http://www.pymol.org).